Optical Materials 140 (2023) 113868

Contents lists available at ScienceDirect

Optical Materials

journal homepage: www.elsevier.com/locate/optmat

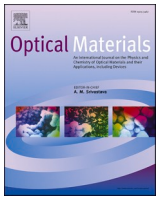

Research Article

# Impact of red emissive ZnCdTeS quantum dots on the electro-optic switching, dielectric and electrochemical features of nematic liquid crystal: Towards tunable optoelectronic systems

Zahra Seidalilir [a,b,*], Sepideh Shishehbor [a], Ehsan Soheyli [c,d], Mohammad Sabaeian [a,b]

[a] Department of Physics, Faculty of Science, Shahid Chamran University of Ahvaz, Ahvaz, Iran
[b] Center for Research on Laser and Plasma, Shahid Chamran University of Ahvaz, Ahvaz, Iran
[c] Department of Physics, Faculty of Science, Ilam University, 65315-516, Ilam, Iran
[d] Department of Electrical-Electronics Engineering, Abdullah Gul University, Kayseri, 38080, Turkiye

ARTICLE INFO

*Keywords:*
Nematic liquid crystal
Quantum dot
Dielectric properties
Electro-optic switching
Electrochemical impedance spectroscopy

ABSTRACT

In the present study, the concentration-dependent dielectric, electro-optical, and electrochemical properties of ZnCdTeS quantum dots (QDs) doped E7 nematic liquid crystal (NLC) mixtures were investigated. The dielectric permittivity components ($\varepsilon_{\parallel}$ and $\epsilon_{\perp}$) and dielectric anisotropy ($\Delta\epsilon = \varepsilon_{\parallel} - \epsilon\perp$) of NLC samples containing varied concentrations of ZnCdTeS QDs (i. e. 0.10, 0.25, 0.50, 0.75, and 1 wt%) were measured at various temperatures. In the nematic phase, the results demonstrated that $\varepsilon_{\parallel}$ increases much more than $\epsilon_{\perp}$ upon an increase in the concentration of ZnCdTeS QDs. $\Delta\epsilon$ enhanced as the concentration of QDs increased, reaching a maximum at 0.50 wt%, then decreased with further addition. Dielectric measurements revealed the formation of self-aligned QD arrays along the nematic director, which act similarly to multiple parallel capacitors in the NLC system. Moreover, electro-optical studies illustrated the significant effect of QDs doping on lowering the threshold voltage and response time. Interestingly, the optical switching-off time of NLC containing 0.50 wt% of the QDs decreased by ~50% compared to that of the pure E7 sample. The reduced screening effect resulting from the QDs ion-capturing mechanism, enhanced effective intermolecular interactions, and increased dielectric anisotropy in the NLC system are the major factors responsible for the improved electro-optical characteristics. The impedance behavior of NLC cells was studied in the frequency range of 0.1 Hz–100 kHz. It indicated that the addition of ZnCdTeS QDs results in a remarkable increase of 96% in the electrical conductivity of the NLC system. Furthermore, the QDs doping significantly improved the NLC device's charge capacitance. Such studies would undoubtedly be beneficial for designing next-generation tunable optoelectronic systems since QDs can be utilized for tuning the dielectric anisotropy, electro-optical characteristics, charge capacitance, and conductivity of NLCs.

## 1. Introduction

Liquid crystals (LCs) are materials having intermediate characteristics between those of liquids and solids, exhibiting the hydrodynamic features of ordinary liquids and the anisotropic properties of crystalline solids [1–3]. In particular, nematic LCs (NLCs) are the most commonly utilized in optoelectronic devices due to their outstanding electro-optical responses as well as lower power consumption [4–7]. In the NLC phase, rod-like mesogens exhibit significant orientational correlation instead of positional correlation. The long molecular axis in this phase tends to align in a direction called the director axis. The nematic director is affected by introducing various anchoring conditions at the substrates or applying an external electric, magnetic, or optical field. The reorientation of molecules in response to the external electric field exceeding a threshold value is known as the Fréedericksz transition [8]; it is the basic theory for applying LCs in display technology.

Different LC operational modes, including vertical alignment [9], fringe-field switching [10], in-plane switching (IPS) [11], and twisted nematic (TN) [12], have been applied to enhance the performance of LCDs. Nevertheless, due to its simple design, acceptable brightness, fast response, and low operation voltage, the TN mode has been the most widely utilized commercial LCD mode [13]. Even though NLCs are the dominating materials in the display industry and switchable optical systems, the performance degradation tendency is a considerable

* Corresponding author. Department of Physics, Faculty of Science, Shahid Chamran University of Ahvaz, Ahvaz, Iran.
*E-mail address:* Z.seidalilir@scu.ac.ir (Z. Seidalilir).

https://doi.org/10.1016/j.optmat.2023.113868
Received 2 February 2023; Received in revised form 29 April 2023; Accepted 1 May 2023
Available online 12 May 2023

challenge for industrial applications [14]. The alignment layer and the NLC mixture used are the two main determinative parameters governing the performance of an NLC device. One of the most critical causes of poor performance for nearly all LCD modes is the existence of ionic impurities within LC devices arising from the LC materials, the alignment layers, the surrounding glue, and the filling procedure [15]. These ions in LCDs can result in image sticking and flickering, an increased threshold voltage ($V_{th}$), and an overall slow response, affecting image quality and switching. Three primary approaches have been adopted to overcome the issues caused by mobile ion impurities. Coating an ion-trapping layer onto the substrate and utilizing a novel NLC compound with a low ionic concentration are two common strategies [16,17]. However, the third approach is modifying the structure of the NLC host by introducing various guest entities, including polymers [18], dyes [19], and nanomaterials [20]. Between these three, the last post-synthesis process is superior in convenience and cost-effectiveness.

Various nanomaterials, including semiconducting nanoparticles (NPs) [20–24], metallic NPs [25], carbon nanotubes [26], and graphene [27], have been utilized to improve the electro-optic switching, dielectric, phase transition, and other characteristics of NLC devices, making NLC mixtures more appropriate for practical applications. The NLC mixture should generally possess a low $V_{th}$, low viscosity, high dielectric anisotropy, and fast switching time. The faster response time and a reduced $V_{th}$ of an NLC by doping the $TiO_2$ NPs were found by Oh et al. [20]. It was reported that doping $Fe_2O_3$ NPs improves the electro-optical and dielectric characteristics of a weakly polar NLC [22]. Singh et al. also found that the presence of gold NPs lowers the nematic-isotropic phase transition temperature and enhances UV–visible absorbance as well as photoluminescence intensity [25]. In a recent work by Lee et al., carbon nanotubes and C60 were incorporated into 5CB or E7-filled NLC devices [26]. The results demonstrate a reduction in the $V_{th}$ and an improvement in the switching performance compared to pure NLC. Additionally, adding graphene flakes into NLCs accelerates the electro-optical switching response considerably [27]. However, the large aggregation of these nanomaterials limits their utilization in LC devices [28].

Quantum dots (QDs) as dopants in LC systems are preferable to other nanomaterials in terms of synthesis, electronic features, and size uniformity. The exceptional quantum confinement and tunable band gap of QDs have boosted attention to their potential applications in various fields like optoelectronics [29], sensing [30], and biomedicine [31]. It has been found that the NLC medium induces the self-assembly of QDs. Basu and Iannacchione revealed by the dielectric characterization that in CdS QD doped 5CB NLC, the QDs are organized into one-dimensional structures parallel to the NLC's director [32]. The formation process of self-assembled QDs in NLCs has been reported by many research groups [33–36]. The high charge transfer features of QDs result in a remarkable interaction among QDs and NLC molecules, which improves the dielectric and electro-optical properties of NLC devices. Self-assembled QD arrays in the NLC cell provide new pathways to facilitate the charge transfer in the system, leading to an increased electrical conductivity in the LC medium [37]. It has been reported that the addition of QDs improves the system's electro-optical response by increasing the LC medium's local polarizability. It becomes possible by the improved pathway of the barrier-free charge transfer of the QDs [38]. Additionally, QDs have been utilized as electron acceptors in organic–inorganic mixtures. The application of an electric field across a QD-doped LC system induces charge transfer from the LC molecules to the QDs, therefore improving the memory characteristics of the LC system [39]. In the NLC mixtures doped with CdSe and CdTe QDs, Kinkead and Hegmann reported that LC-QD combinations can exhibit different alignment and electro-optical properties based on the size, capping agent, and percentage of the QDs. They demonstrated that introducing these QDs to the NLC reduces the host's threshold voltages, rise time, and splay elastic constant [40]. Cho et al. found a significant decrease in $V_{th}$ (14.8%), falling time (30%), and rising time (63.6%) of TN cells upon doping with graphene QDs [41]. Rastogi et al. investigated the memory response of NLCs doped with $Cd_{1-x}Zn_xS/ZnS$ QDs using dielectric and electro-optical measurements; Doping the QDs resulted in a significant increase in the memory parameter of NLC [42]. Recently, we demonstrated that Ni:ZnCdS/ZnS QDs improve the charge transport as well as the bulk and double-layer capacitance of E7 NLC considerably [37]. Furthermore, these QDs enhance the dielectric anisotropy of the NLC device while reducing its $V_{th}$. Such multifunctional QDs can potentially improve the electro-optical response of NLCs, resulting in more successful research in LC-based nanoscience and nanotechnology. Therefore, it would be advantageous to conduct an in-depth study on QD-NLC composites to investigate the tunability of various physical features of doped NLC mixtures, which would ultimately benefit a wide range of optoelectronic systems.

In this work, the impact of ZnCdTeS QDs on temperature-dependent dielectric anisotropy, $V_{th}$, switching-on and switching-off response times, and rotational viscosity is discussed in detail. An impedance spectroscopy study is also performed to investigate the electrophysical features of QD doped NLC samples in the bulk and near-alignment areas. The electrical conductivity, capacitance, ion mobility, and ion diffusion of NLCs containing various amounts of QDs are investigated. To the best of our knowledge, there is no report on using luminescent ZnCdTeS QDs as dopants to improve the electrochemical and electro-optical features of an NLC system. The results demonstrate that the addition of ZnCdTeS QDs significantly enhances the electro-optical response, electrical properties, and charge capacitance of E7 NLC. This research will be beneficial for the applications of optoelectronic systems.

## 2. Experimental details

### 2.1. NLC material used

The host NLC utilized in this investigation is the E7 eutectic mixture (Merck). This multi-component eutectic NLC mixture consists of four cyanoparaphenylene derivatives: 51 wt% of 4-cyano-4′-pentylbiphenyl, 25 wt% of 4′-heptyl-4-biphenylcarbonitrile, 16 wt% of 4′-n-oxyoctyl-4-cyanobiphenyl, and 8 wt% of 4-cyano-4″-n-pentyl-terphenyl [43]. The birefringence of E7 NLC is approximately 0.21 at 27 °C, and its nematic-isotropic phase transition temperature is around 61 °C [37,43]. Because of its superior stability and high dielectric anisotropy at application-typical temperatures, the E7 mixture has attracted much attention in the theoretical and experimental investigations on NLCs [43,44].

### 2.2. Preparation and properties of ZnCdTeS QDs

The red-emitting ZnCdTeS QDs used in this study have been prepared via a colloidal reflux method in a basic reaction medium based on our previous study [45]. Typically, specific amounts of $ZnCl_2$, CdOAc, N-acetyl-L-cysteine (NAC), and trisodium citrate were dissolved in 100 mL of deionized water. After it, the solution's pH was fixed at 11.4 to reach red-emitting QDs. After transferring to a 3-necked/round bottom flask, freshly prepared NaHTe (by reducing Te in an excess amount of $NaBH_4$ in deionized water) was quickly injected into the stirring reaction solution (the nominal molar ratios of precursors were Cd:Zn:NAC:SC:Te = 1:1.5:0.9:0.7:0.36). Finally, the reaction solution was heated to 100 °C and refluxed for 2 h. The finalized QDs in colloidal form were purified using an excess amount of acetone and centrifugation at 4000 rpm for 15 min to make them suitable for further optoelectronic measurements. After a two-step washing process, they were dried overnight at room temperature. The average particle size of the synthesized QDs was ~4 nm. As mentioned earlier [45], the PL emission peak is located at around 618 nm with strong red emission and full-width at half maximum of about 52 nm, which all are promising results for such a simple and low-cost method, showing the excellent efficiency of the synthesis approach. The red emissive QDs were selected due to their narrower

bandgap energy and ability to be excited at longer wavelengths, facilitating interaction with NLC under a specific external field.

### 2.3. Preparation of the LC sample cells

Throughout this study, planar (homogeneous), TN, and homeotropic NLC cells were made to investigate various characteristics of NLC samples. Each LC cell comprises NLC material sandwiched between two indium-doped tin-oxide (ITO) glass substrates (typically $1.0 \times 1.5$ cm$^2$). The planar alignment is achieved by covering these glass plates with a layer of polyvinyl alcohol (PVA), followed by unidirectional mechanical rubbing with a soft cloth to obtain a high-quality, uniform alignment for NLC molecules. Similarly, glass substrates are coated with PVA and rubbed in one direction for TN alignment. However, the rubbing directions on two ITO glasses are perpendicular, resulting in a 90-degree twist of the director from one surface to the other within the cell. For setting the homeotropic alignment, the ITO-coated substrates are treated with lecithin to align the LC molecules perpendicular to the surface of the glass plates [37,46]. For planar and homeotropic cells, the cell gap is fixed at 25 μm, whereas for TN cells, it is maintained at 9 μm. Using an optical technique based on the interference patterns of light reflected from the glass electrodes in each empty cell, the cells thickness was determined. ZnCdTeS QDs powder is disseminated in ethanol and sonicated for 5 h to make a homogeneous solution. Then, various amounts of the produced solutions are added to E7 to make NLCs comprising 0.10, 0.25, 0.50, 0.75, and 1 wt% of the QDs. The mixtures are sonicated in an ultrasonic bath for 6 h while heated to achieve a uniform mixture. The ethanol applied to disperse QDs evaporates by placing the solution in a vacuum heat chamber at 90 °C. In the isotropic phase, NLCs containing different concentrations of QDs are capillary injected into cells. A polarized optical microscope (POM) is utilized to investigate the dispersion uniformity of QDs in NLC material and the alignment homogeneity of NLC samples. The electric field is perpendicularly introduced to the NLC device's surface during all characterizations.

### 2.4. Characterization techniques

The dielectric investigations were performed utilizing an LCR meter (Instek LCR-8110G) with an accuracy of 0.005 and a cell temperature controller with a precision of 0.01 °C. The LCR meter functioned in parallel equivalent circuit mode at 10 kHz with a sinusoidal probe voltage of 100 mV, significantly below the NLC samples' $V_{th}$. For each NLC material, $\varepsilon_{\parallel}$, the parallel dielectric permittivity component, was obtained using a homeotropic cell. In contrast, the perpendicular component, $\varepsilon_{\perp}$, was achieved by employing a cell with planar alignment. The capacitance values of both filled and empty cells were determined at various temperatures. The proportion of filled capacitance to empty capacitance was calculated to obtain the values of the dielectric permittivities of NLC samples [23]. The transmittances versus wavelength of pure and ZnCdTeS QDs doped NLC samples were measured using a UV-spectrometer (Specord S600, Analytik Jena) to investigate the transparency of the NLC materials. As an incident light source, a He–Ne laser (5 mW; 632 nm) was utilized to obtain the electro-optical characteristics of the prepared TN LC samples. The laser light falls of normal incidence on the TN cells placed between a pair of cross-polarizers. The transmitted light was monitored as a function of the voltage applied to TN cells or time using a photodiode connected to an oscilloscope. A DC square-wave voltage of 10 V (much higher than $V_{th}$) was applied to the cells to measure the time-dependent transmittance variation. The electrochemical characteristics of NLC samples were investigated utilizing electrochemical impedance spectroscopy (EIS) data examined using an Autolab PGSTAT302 N impedance analyzer with a frequency accuracy of 0.003%. EIS measurements were performed on pure and QDs doped planar cells under an excitation amplitude of 100 mV, which was substantially below the Freedericksz $V_{th}$, over the frequency range of 100 mHz–0.1 MHz and at the temperature of 298 K. The EIS data were fitted to an appropriate electrical equivalent circuit (EEC) model utilizing Z-view software.

## 3. Results and discussion

### 3.1. Dielectric study

The impact of ZnCdTeS QDs on the molecular interactions in the NLC matrix can be better understood using dielectric measurements. Fig. 1 demonstrates the temperature-dependent components of dielectric permittivity along and perpendicular to the nematic director for pure E7 and ZnCdTeS QDs doped NLC samples at 10 kHz. The dielectric permittivity components of NLC mixtures can be split into sections associated with the nematic ($\varepsilon_{\parallel}$ & $\varepsilon_{\perp}$) and isotropic ($\varepsilon_{iso}$) phases. Main factors responsible for the temperature-dependent dielectric behavior of nanomaterial doped nematic systems are the shape and concentration of nano-dopants as well as the mutual interaction between nano-dopants and LC molecules [46]. For all NLC samples, the value of $\varepsilon_{\perp}$ increases while $\varepsilon_{\parallel}$ exhibits a decreasing trend with temperature. The behavior of pure E7 NLC dielectric components at various temperatures is consistent with the previous reports [37,47].

At 25 °C, when the concentration of ZnCdTeS QDs rises, the value of $\varepsilon_{\perp}$ increases in a systematic manner. $\varepsilon_{\parallel}$ of NLC devices rises with the addition of ZnCdTeS QDs up to 0.50 wt% and subsequently declines when the amount of QDs is increased further. Results reveal that in the nematic phase, adding ZnCdTeS QDs to the NLC results in a higher increase in the value of $\varepsilon_{\parallel}$ than $\varepsilon_{\perp}$. Fig. 2a depicts the temperature-dependent dielectric anisotropy $\Delta\varepsilon$ for ZnCdTeS QDs doped NLC cells at the frequency of 10 kHz. In the nematic phase, when QDs are added to the NLC, $\Delta\varepsilon$ increases to attain a maximum at 0.50 wt%, then decreases with further increased concentration, as illustrated in Fig. 2b. The alignment states of NLC cells as a function of the doping concentration of ZnCdTeS QDs were investigated using the POM images (Fig. S1). Uniform LC alignments were obtained, indicating that the alignments were created correctly and the ZnCdTeS QDs were dispersed uniformly in the LC medium. When up to 0.50 wt% of ZnCdTeS QDs is added to the NLC, small aggregations appear that are difficult to see with the naked eye; however, more aggregations are appeared at concentrations greater than 0.75 wt%.

It is worth mentioning that the polarity and orientation of the molecules are two primary factors in investigating the dielectric behavior of

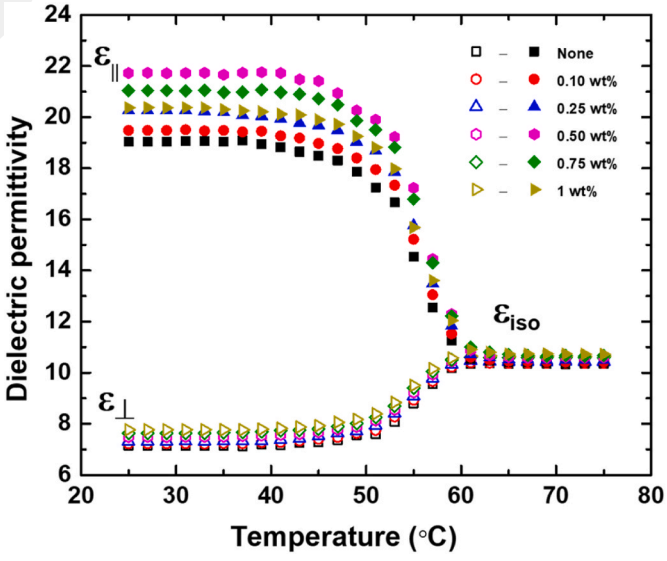


**Fig. 1.** Temperature-dependent parallel and perpendicular components of dielectric permittivity of NLC samples containing varied concentrations of ZnCdTeS QDs.

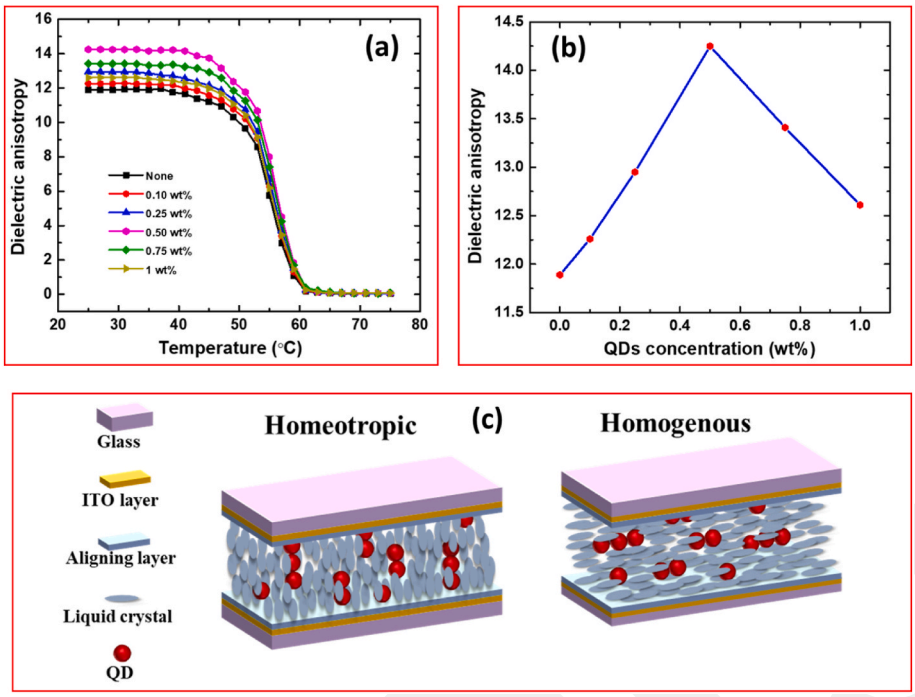


**Fig. 2.** (a) Temperature-dependent dielectric anisotropy for NLC samples containing varied concentrations of ZnCdTeS QDs, (b) the changes in dielectric anisotropy as a function of the QDs concentration at 25 °C, and (c) schematic representation of directed self-assembled QD arrays in homogeneous (planar) and homeotropic NLC cells.

the NLCs. Adding nano-dopants to an orientated NLC system can modify these factors. Therefore, it is crucial to consider the dielectric permittivity of nanomaterials and their effect on the orientation of the NLC molecules. If the dielectric permittivity of the nano-dopant is greater than that of the NLC, nanomaterial addition will increase the dielectric permittivity of the doped NLC mixture. Although ZnCdTeS QDs possess a smaller dielectric permittivity than the E7 NLC, the presence of QDs enhances the dielectric coefficients of QDs-NLC mixtures. On the other hand, individual QDs in an NLC medium do not exhibit dielectric anisotropy due to their spherical shape. According to the previous reports [32,36], the excluded volume must be minimized to decrease the free energy in a QD–LC system. Consequently, QDs effectively interact in the LC bulk to create arrays in a single direction parallel to the nematic director. The appropriate ordering and geometrical summation of the dielectric permittivity value of each ZnCdTeS QD in the aligned arrangement of the NLC will enhance dielectric permittivity in the QD–NLC samples. Our dielectric results confirm the formation of such QD arrays in the LC device. Due to their one-dimensional structure, self-aligned QD arrays are expected to behave similarly to multiple parallel capacitors, creating an additional dielectric anisotropy in the LC medium. Fig. 2c schematically depicts the possible formation of these self-assembled QD arrays in the homogenous and homeotropic NLC cells. For homeotropic cells, when up to 0.50 wt% of QDs are added, the QD arrays exhibit homeotropic alignment within the system and contribute their average parallel dielectric permittivity $\varepsilon_{\parallel}$ (which is higher than $\varepsilon_{\perp}$) to the NLC system, thereby increasing $\varepsilon_{\parallel}$. At higher concentrations, however, QD aggregations cause local random disorders in the system and prevent a number of NLC molecules from aligning completely homeotropically in the cell, resulting in a decrease in the mean $\varepsilon_{\parallel}$ of the system. QD arrays exhibit planar alignment for planar cells and contribute their average perpendicular dielectric permittivity to the system, leading to an increase in $\varepsilon_{\perp}$. Planar-configured NLC molecules, which are perpendicular to the electric field, possess the lowest dielectric permittivity, $\varepsilon = \varepsilon_{\perp}$. Therefore, if the NLC molecules deviate from their precisely aligned state in the planar cell, the system's dielectric permittivity will increase. At QD concentrations greater than 0.50 wt%, where QD aggregations begin, a portion of molecules lose their planar arrangement within the cell, resulting in a rise in the dielectric permittivity. Thus, $\varepsilon_{\perp}$ increased systematically with increasing QD concentration up to 1 wt%. The difference between $\varepsilon_{\perp}$ of the sample containing 0.50 wt% of QDs and that of the pure E7 sample is 0.35. Wheras, the addition of 0.50 wt% QDs increases $\varepsilon_{\parallel}$ of the system by an amount of 2.70. The noticeable difference between $\varepsilon_{\perp}$ and $\varepsilon_{\parallel}$ variations confirms the formation of one-dimensional arrays along the nematic director. If the distribution of particles in the system were random, no difference between $\varepsilon_{\perp}$ and $\varepsilon_{\parallel}$ variations would be expected.

In addition to the self-aligned QD arrays, the dipolar interaction mechanism between NLC and QD molecules can also lead to an increased dielectric anisotropy. The dipolar interactions among NLC molecules and ZnCdTeS QDs appear to enhance with the introduction of the QDs up to 0.50 wt%, leading to an increase in the system's dielectric anisotropy. Three kinds of interaction maytake place in the NLC samples: (i) NLC–NLC interaction, (ii) NLC–QD interaction, and (iii) QD–QD interaction. The dominating interaction depends on the concentration of the QDs. While in pure E7 NLC, only interactions between NLC molecules occur, the other two interactions are included upon introducing the QDs into the NLC. When 0.50 wt% of QDs is added, the NLC–QD interaction appears more dominant than NLC–NLC and QD–QD interactions. However, the QD–QD interaction dominates upon further addition of the QDs, probably leading to the aggregation of QDs in the NLC. On the other hand, ionic impurities in NLC samples might behave as guest particles and deform the LC molecule's orientation, affecting the systems' order. $\Delta\epsilon$ is straightly related to the order parameter [48]; therefore, an increase in the order parameter will result in higher $\Delta\varepsilon$ in the NLC system. When ZnCdTeS QDs are added into NLC, the ionic impurities concentration decreases by adsorbing the ions on the surface of QDs, increasing the order parameter and, therefore, $\Delta\varepsilon$ of the NLC sample. However, at higher concentrations, the aggregation impact of QDs can dominate the ion-capturing effect, leading to a decreased order parameter. Table 1 lists the dielectric anisotropy of samples in the nematic phase (recorded at T = 25 °C). The dielectric anisotropy of the pure E7 NLC device is 11.89. The value of $\Delta\varepsilon$ increases to 14.25 on

**Table 1**
Measured dielectric anisotropy ($\Delta\varepsilon$), the threshold voltage ($V_{th}$), the switching-on time ($\tau_{on}$), the switching-off time ($\tau_{off}$), and estimated splay elastic constant ($K_{11}$) and rotational viscosity ($\eta$) of NLC samples containing varied concentrations of ZnCdTeS QDs at the temperature of 25 °C.

| samples | $\Delta\varepsilon$ | $V_{th}$ (V) | $K_{11}$ ($10^{-11}$ N) | $\tau_{on}$ (ms) | $\tau_{off}$ (ms) | $\eta$ (mPas) |
|---|---|---|---|---|---|---|
| None | 11.89 | 2.56 | 6.99 | 4.81 | 13.91 | 15.36 |
| 0.10 wt% QDs | 12.26 | 2.41 | 6.39 | 4.70 | 10.49 | 10.59 |
| 0.25 wt% QDs | 12.95 | 2.36 | 6.47 | 4.18 | 8.16 | 8.34 |
| 0.50 wt% QDs | 14.25 | 2.22 | 6.30 | 3.24 | 6.89 | 6.86 |
| 0.75 wt% QDs | 13.41 | 2.30 | 6.37 | 3.42 | 7.08 | 7.13 |
| 1 wt% QDs | 12.61 | 2.52 | 7.19 | 3.94 | 12.57 | 14.28 |

adding ZnCdTeS QDs (0.50 wt%) to the NLC, while the dielectric anisotropy decreases to 12.61 at 1 wt%. Such a significant increase in dielectric anisotropy in the presence of a relatively small amount of QDs would undoubtedly benefit low-power NLC-based electro-optical devices.

Besides, the $\Delta\varepsilon$ value of the NLC samples decreases with an increase in temperature. In this case, the system's disorder rises at elevated temperatures, resulting in a reduced difference between $\varepsilon_{\parallel}$ and $\varepsilon_{\perp}$ and subsequent a reduction in dielectric anisotropy close to the phase transition temperature, as Fig. 2a shows. In the isotropic phase, $\Delta\varepsilon$ of the NLC samples approaches zero, as expected. Therefore, the system's order parameter decreases to zero, and the QDs are uniformly scattered within the system. In other words, self-aligned QD arrays collapse as the temperature increases, and QDs become uniformly dispersed in the system. According to the obtained results, the clearing point of the NLC samples is not affected by the addition of ZnCdTeS QDs. The nematic-isotropic phase transition temperature ($T_{N\text{-}I}$) of NLC samples containing varied concentrations of ZnCdTeS QDs was measured using differential scanning calorimetry (DSC) at a scan rate of 5 °C/min (Fig. S2). $T_{N\text{-}I}$ remains nearly unchanged upon the inclusion of ZnCdTeS QDs, consistent with the dielectric results. Notably, explaining the impact of doping nanostructures on $T_{N\text{-}I}$ of NLCs may be challenging. $T_{N\text{-}I}$ is influenced by the nanodopant's chemical structure, shape, size, ligands, permanent polarization, and anchoring interactions between nanostructure and the NLC molecules. The used QDs have a spherical shape, which differs from the shape of LC molecules. Anchoring interactions between the NLC molecules and the nanodopants result in a reduction in $T_{N\text{-}I}$, while the permanent polarization of the nanostructures is a factor that contributes to an increase in $T_{N\text{-}I}$. In this work, we believe that the system's $T_{N\text{-}I}$ with the addition of ZnCdTeS QDs is constant as a result of the net effect of these major competitive effects.

### 3.2. Electro-optical study

For electro-optical measurements, a laser beam with a wavelength of 632 nm was employed; hence, the samples' transparency should be checked at this wavelength. Fig. 3 shows the transmittance spectra of NLCs containing different concentrations of ZnCdTeS QDs over the wavelength range of 350–750 nm. At the wavelength of 632 nm, the optical transmittance of samples remains nearly constant upon adding ZnCdTeS QDs up to 0.50 wt% and slightly lowers with additional introduction of QDs. It can be attributed to the light scattering caused by the aggregation of ZnCdTeS QDs. The average transmittance value of the NLC mixtures is 83.31% at the wavelength of 632 nm.

The designed structure of the TN LC cell placed between two crossed polarizers is shown in Fig. 4. Because of the orthogonal anchoring orientations on the ITO substrates, the long axis of the NLC molecules in a natural state cell twists by 90° from one substrate to another. Therefore, as shown in Fig. 4a, in the TN LC, the direction of beam light's

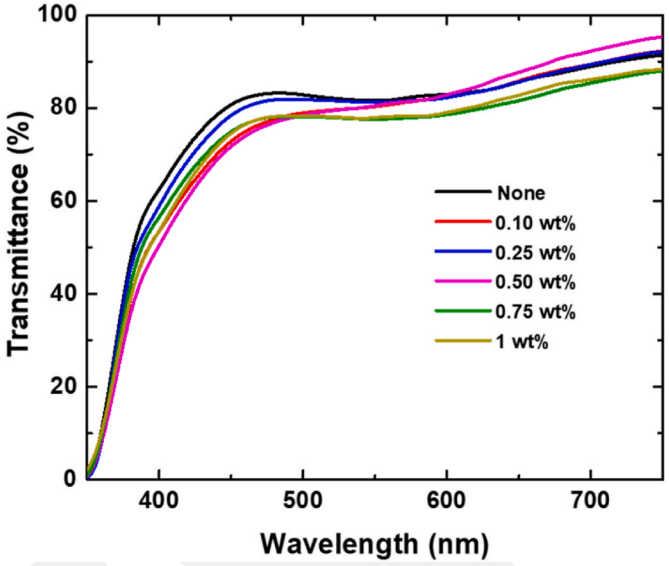


**Fig. 3.** Optical transmittance spectra of NLC samples containing different concentrations of the ZnCdTeS QDs as the function of wavelength at 25 °C.

polarization rotates by 90°, allowing it to pass through the second polarizer. When an electric field (stronger than the threshold switching value) is supplied to the TN cell, the NLC molecules rotate and align along the electric field's direction, as illustrated in Fig. 4b. Therefore, the second polarizer blocks the emergent light because the incident light' polarization direction remains unchanged.

Fig. 5 illustrates the normalized transmittance as a function of voltage (V-T) for TN samples containing varied concentrations of ZnCdTeS QDs at 50 Hz and the temperature of 25 °C. The $V_{th}$ of the normally white TN mode cell is the voltage at which the light transmittance drops to 90% of its initial value at zero voltage [37,49]. As depicted in the inset of Fig. 5, $V_{th}$ of the NLC cell drops upon the addition of the QDs. Table 1 presents the $V_{th}$ values of TN LC samples containing varied amounts of the QDs at 25 °C. $V_{th}$ is 2.56 V for the pure NLC sample, consistent with the values reported in the literature for pure E7 [27,37]. The value of $V_{th}$ decreases as the concentration of QDs rises to 0.50 wt%, while it increases with further addition. This decrease in $V_{th}$ implies that lower voltage is required to reorient molecules in ZnCdTeS QDs doped LC devices, which is advantageous for low-power display technology. In the LC sample, the splay elastic coefficient $K_{11}$ could be examined, but the twist and bend elastic coefficients $K_{22}$ and $K_{33}$, respectively, can be ignored. According to the Freedericksz transition experiment [50], $V_{th}$ is linked to $K_{11}$ by:

$$V_{th} = \pi\sqrt{\frac{K_{11}}{\varepsilon_0 \Delta\varepsilon}} \quad (1)$$

in which $\varepsilon_0$ is the permittivity of free space. Thus, $K_{11}$ can be determined by measuring $V_{th}$ and $\Delta\epsilon$. As demonstrated in Table 1, $K_{11}$ declines as the concentration of QDs rises to 0.5 wt% but increases with an additionally increased concentration of the QDs.

Fig. 6 illustrates the time-dependent transmittance intensity of TN LC samples when the applied field is switched on and off. The switching-on time, $\tau_{on}$, is expressed as the time required for the TN cell transmittance to fall from 90% to 10% of the highest transmission after the introduction of voltage (off-on state) [51]. Fig. 6 indicates that the cell transmittance rises with time when the applied voltage is switched off (on-off state). The switching-off time, $\tau_{off}$, is the time required for the TN cell transmittance to increase from 10% to 90% of the highest transmission after the voltage is switched off [51]. The switching-on time corresponding to reorientation forced by the electric field is shorter than the switching-off time related to spontaneous relaxation reorientation.

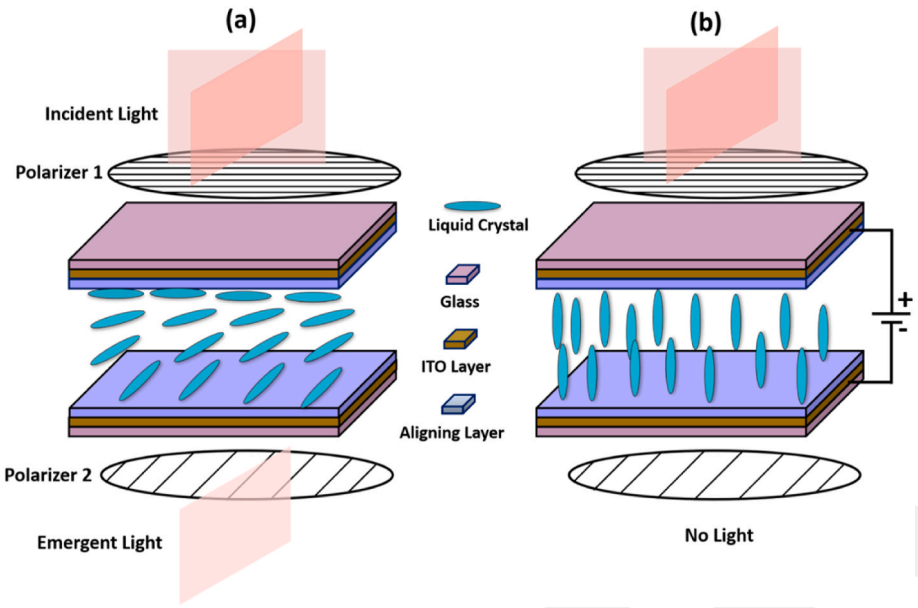


**Fig. 4.** Schematic representation of the TN LC cell located between two linear polarizers. (a) The incident light is transmitted through the normally twisted configuration, or (b) it is obstructed by an applied voltage (more than the threshold voltage).

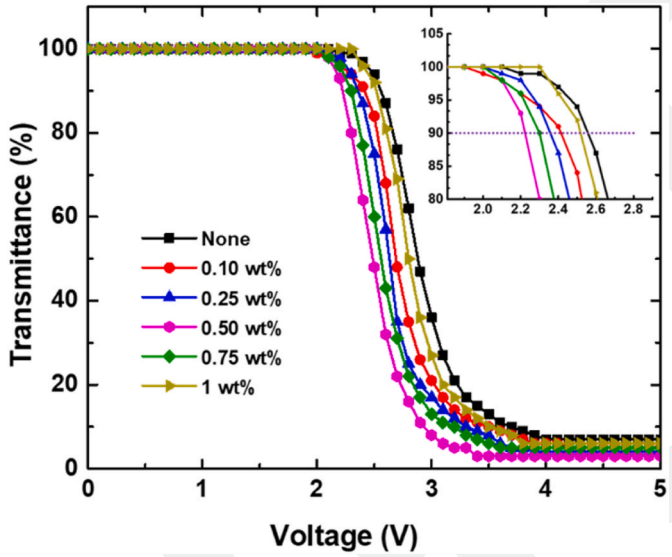


**Fig. 5.** Voltage-dependent optical transmittance for TN LC samples containing varied concentrations of ZnCdTeS QDs at 50 Hz and the temperature of 25 °C. The inset displays an expanded view of V-T curves close to the transmittance of 90%.

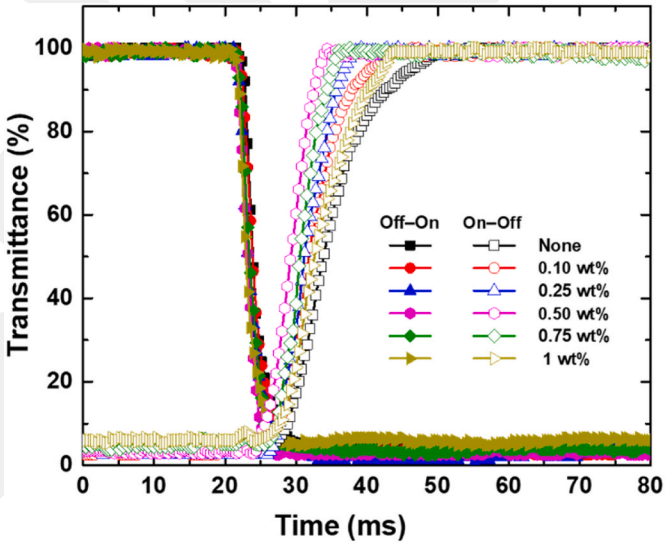


**Fig. 6.** Time-dependent optical transmittance for TN LC cells containing varied concentrations of ZnCdTeS QDs at 25 °C.

Table 1 lists the values of $\tau_{on}$ and $\tau_{off}$ for TN LC samples containing varied amounts of the QDs at 25 °C. $\tau_{on}$ and $\tau_{off}$ for the pure NLC sample are 4.81 ms and 13.91 ms, respectively, comparable to the values reported for pure E7 [52]. However, when ZnCdTeS QDs are added to the NLC, $\tau_{on}$ decreases to a minimum of 3.24 ms at 0.50 wt% but increases with further increased concentration. The variations of $\tau_{off}$ as a function of the QDs concentration reveal a similar trend. For the NLC cell with 0.50 wt% ZnCdTeS QDs, the measured $\tau_{off}$ is 6.89 ms, which is approximately 50% of the value obtained for the pure NLC.

The two characteristic electro-optical response times, $\tau_{on}$ and $\tau_{off}$, of the nematic director, can be defined as [53]:

$$\tau_{on} = \frac{\eta d^2}{\Delta\varepsilon\varepsilon_0 V^2 - K_{11}\pi^2}, \tau_{off} = \frac{\eta d^2}{K_{11}\pi^2} \quad (2)$$

where $\eta$ denotes the LC rotational viscosity, $V$ applied voltage, and $d$ is the thickness of NLC cell. The NLC rotational viscosity illustrates the friction between LC molecules in the rotation procedure. We expect increased dielectric anisotropy, enhanced NLC-QDs intermolecular interactions, and decreased LC rotational viscosity to be factors responsible for the significantly reduced $\tau_{on}$ and $\tau_{off}$. Due to the presence of functional groups such as –CN (hydrogen bond acceptor group) in E7 NLC and the chemical structure of the synthesized QDs, it is expected that hydrogen bonds exist between LC molecules and QD molecules. Consequently, hydrogen-bonded intermolecular interactions will be expected between QDs and LC molecules, as well as between QDs themselves.

The presence of QDs as external additives may increase internal friction and, therefore, rotational viscosity $\eta$, while the reduction of ionic impurities decreases $\eta$. The effect of these competitive factors on the electro-optical responses of the NLC samples is schematically

represented in Fig. 7. When an electric field ($E$) over the threshold switching value is applied to the cell, the nematic system faces a torque proportional to $\Delta\varepsilon E^2$ [54]; therefore, the nematic director can reorient parallel to the electric field. As shown in Fig. 7a, positive and negative ions can move toward electrodes in the presence of an electric field, creating an ion current in the cell. For the pure NLC sample, transport of the ionic impurities causes high internal friction among LC directors, leading to a slow electro-optical response. The collected ionic impurities on the electrodes generate an internal electric field, hence decreasing the effective voltage applied to the LC samples. Because of the screening effect, the $V_{th}$ of the TN LC cell increases.

The dispersed ZnCdTeS QDs reduce the ion transport and ion accumulation on the substrate surfaces by trapping some concentration of mobile ions, as depicted in Fig. 7b. The decreased screening effect caused by the accumulated ionic impurities can be a crucial factor for the $V_{th}$ reduction. Swiping the mobile ions, on the other hand, reduces $\eta$, hence quickening the electro-optical response of the nematic switching. According to the electro-optical results, the ionic impurities reduction is dominant when QDs up to 0.50 wt% are introduced to E7 NLC. With a further increase in QDs concentration, the presence of QDs as external additives in the system overcomes the effect of ionic impurity reduction. Indeed, if a high concentration of QDs is used, aggregation occurs in the NLC medium, resulting in a reduced QDs effective surface area for ion trapping, as shown in Fig. 7c. Aggregation of QDs increases rotational viscosity in the system and, consequently, slows the electro-optical response of nematic switching. The optimum weight percentage of ZnCdTeS QDs in an NLC mixture was determined to be 0.50 wt% from an applied perspective. $\eta$ of NLC samples is obtained using Eq. (2) for $\tau_{off}$ and is listed in Table 1 $\eta$ of the sample of pure E7 NLC is 15.36 mPas. However, the value of $\eta$ decreases when ZnCdTeS QDs are added and reaches 6.86 mPas at 0.50 wt%, whereas it increases when the quantity of QDs is increased further.

### 3.3. Electrochemical study

The electrochemical impedance spectroscopy technique is valuable for evaluating the carrier transport mechanism and capacitive features in solid and liquid materials' bulk and interface areas [55]. Various electrophysical characteristics of the NLC samples are obtained using this technique. The magnitude of overall impedance (OI) and dielectric loss tangent are the main parameters that are expressed, respectively, as [56]:

$$|Z| = \sqrt{Z'2 + Z''2} \tag{3}$$

$$\tan\varphi = \frac{Z'}{Z''} \tag{4}$$

which involve real $Z'$ and imaginary $Z''$ components of the impedance. Fig. 8a depicts the frequency-dependent OI of NLC samples containing various concentrations of ZnCdTeS QDs at 25 °C. The variation trend of OI with increasing frequency for the pure E7 sample is consistent with the results previously reported [37,57]. The value of OI for undoped E7 NLC exhibits a decreasing trend with an increase in frequency up to 37 Hz. Afterward, it remains consistent as the frequency increases to approximately 350 Hz. The OI value then decreases linearly as the frequency increases to 14 kHz. It drops gradually over 14 kHz, eventually attaining a horizontal asymptote. Similar behavior is observed for the OI of dispersed NLC samples with increasing frequency. However, in the low-frequency region, the doped NLCs demonstrate a minor shift toward lower frequencies compared to the pure E7 NLC.

The value of OI reduces when ZnCdTeS QDs are introduced up to 0.50 wt%, but rises as additional QDs are added. $\tan(\varphi)$ represents the dielectric loss or the power lost by an applied AC voltage inside a dielectric material. The frequency-dependent dielectric loss tangent of NLC samples containing varied concentrations of ZnCdTeS QDs is illustrated in Fig. 8b. The absolute value of $\tan(\varphi)$ increases with increasing frequency, attains a maximum at the saddle point frequency of the OI and then declines. At $f_{peak}$, the highest dielectric loss occurs when the applied electric field polarity changes slowly enough to enable the free ions to travel toward the electrodes with opposite charges. In this frequency regime, a space charge forms close to the interface, increasing the cell's capacitance [57–59]. The real and imaginary parts of impedance decrease as the concentration of QDs rises up to 0.50 wt% but increase at higher concentrations (Fig. 8c and d).

Fig. 9 depicts the impedance Nyquist plots, which are the imaginary part against the real part, of NLCs containing various concentrations of QDs. Different electrophysical parameters can be obtained by modeling the impedance data as a combination of cell resistance and capacitance. Various equivalent electrical circuits (EECs) for modeling NLC cells have been reported. Garcia et al. introduced a primary EEC including a parallel collection of NLC resistance, $R_{LC}$, and NLC capacitance, $C_{LC}$, corresponding respectively to the active and reactive manners of the NLC, in series with a resistance, RCR, representing the resistivity of the outer elements and cell electrodes connections [60]. This simplified model, utilized for NLC doped with multi-walled carbon nanotubes, is correct for materials with low conductivity and a frequency range from 100 Hz to 100 kHz. For modeling both high- and low-frequency behaviors of the NLC samples or the samples with moderate conductivity, Sprokel presented an EEC consisting of double-layer capacitance, $C_{DL}$, in series with the paralleled set of $C_{LC}$ and $R_{LC}$ [61]. By inserting $C_{DL}$, the possible formation of space-charge regions close to the electrodes, resulting from the confinement effect in an NLC sample, is regarded. Afterward, the EEC was expanded by employing a Warburg element $W$ to describe the charge transport process in an NLC system [56]. The EEC model utilized in this study, a mix of the three formerly discussed models, is illustrated

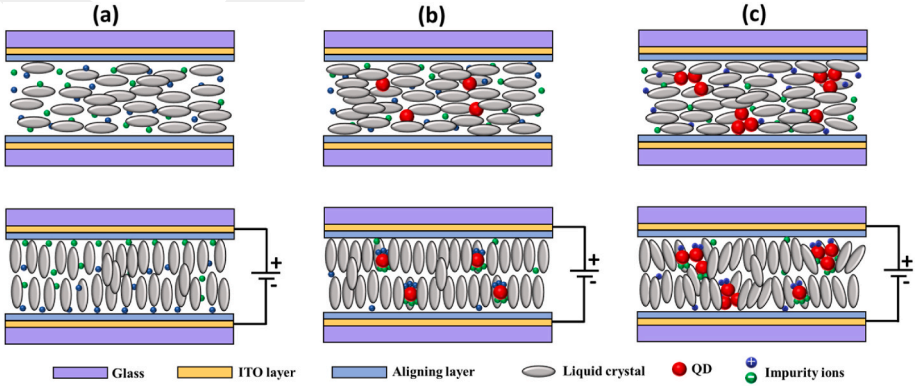


**Fig. 7.** Schematic representation of (a) pure NLC cell, (b) NLC cell containing ZnCdTeS QDs at optimum concentration, and (c) NLC cell containing higher QDs concentration before and after applying an electric field greater than the threshold switching value.

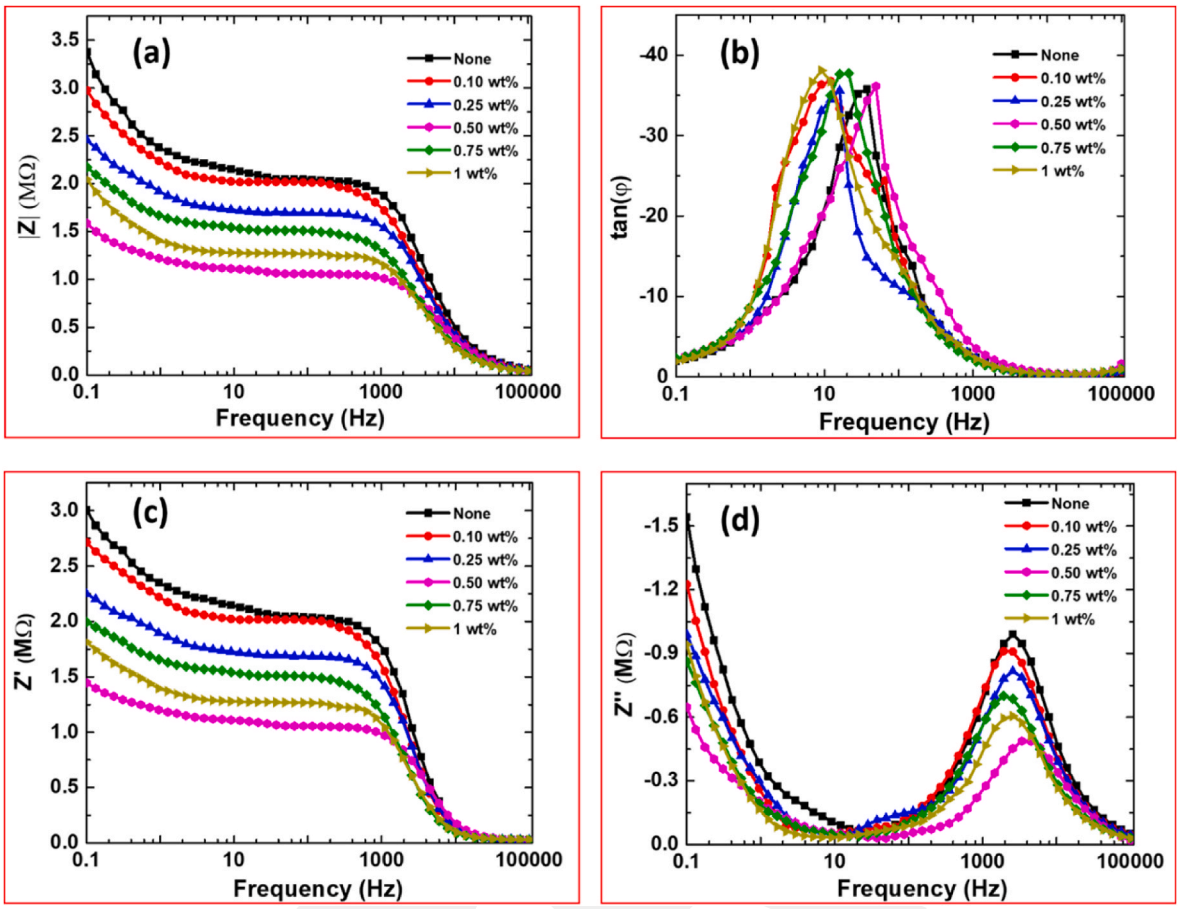


**Fig. 8.** Overall impedance (a), dielectric loss tangent (b), the real component of impedance (c), and imaginary component of impedance (d) for NLC cells containing varied concentrations of the red emissive ZnCdTeS QDs at 25 °C.

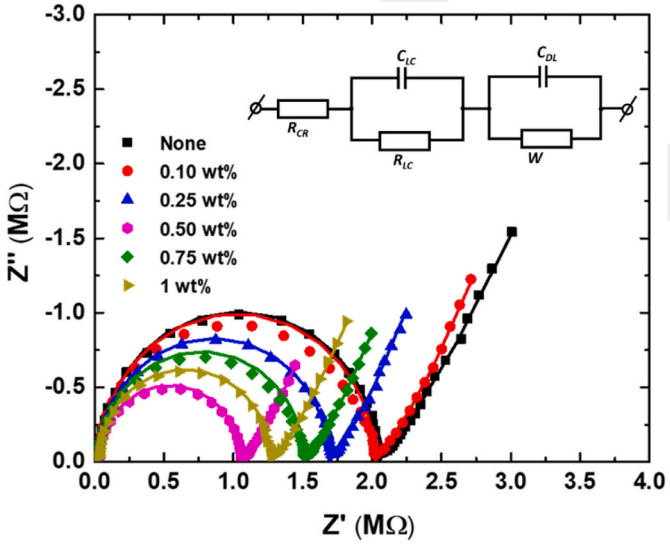


**Fig. 9.** Nyquist curves of NLCs containing varied concentrations of ZnCdTeS QDs at 25 °C. Symbols represent the measured value, while solid curves represent the results of simulation based on the equivalent circuit model displayed in the inset.

in the inset of Fig. 9. It should be noted that $C_{LC}$ is attributed to the perpendicular dielectric permittivity component, $\varepsilon_{\perp}$, whereas $R_{LC}$ is related to residual impurities. Consequently, $R_{LC}$ can be considered a measurement of the sample's conductivity. For modeling the impedance behavior in the low-frequency region, the ion drift and space charge accumulation close to the electrodes must be taken into account [56,58]. It was reported that in the high-frequency regime, the polarity changes too quickly for the ions to react; as a result, there are no formed space charges around the electrodes [58]. The Warburg impedance is given by Ref. [62]:

$$Z_w = \frac{w_{sr}}{\sqrt{\omega}}(1-j)\tanh\left(w_{sc}\sqrt{j\omega}\right) \tag{5}$$

in which $w_{sr}$, bulk Warburg coefficient, and $w_{sc}$, double-layer Warburg coefficient, can be expressed as below:

$$w_{sr} = \frac{RTN_A}{F^2 B n_s \sqrt{2D}} \tag{6}$$

$$w_{sc} = \frac{\delta_N}{\sqrt{D}} \tag{7}$$

in which appear temperature $T$, gas constant $R$, Avogadro's constant $N_A$, Faraday' constant $F$, the surface area of sample $B$, the concentration of the mobile ions $n_s$, the mobile ions effective diffusion coefficient $D$, and the Nernst diffusion layer thickness $\delta_N$. In Fig. 9, symbols indicate the experimental data, while solid curves depict the highly accurate simulation findings achieved by using the EEC model. For all Nyquist curves, the semicircle at the high-frequency region represents the charge transport resistance and the bulk NLC capacitance. In contrast, a sloping line at the low-frequency region reveals mobile ion diffusion and NLC double-layer capacitance. The semicircle's edge and diameter reflect $R_{CR}$ and $R_{LC}$, respectively [56,58,63]. The deviation of the semicircle centers from the real axis in Nyquist plots implies a non-Debye type

relaxation in the NLC mixtures. Table 2 lists the data obtained for the EEC model components $R_{LC}$, $C_{LC}$, $C_{DL}$, and $W_{sr}$ associated with the best fit.

Various physical parameters, including electrical conductivity, mobility and diffusion coefficient of ions, and thickness of the Nernst layer, are derived utilizing simulation-obtained direct data. The electrical conductivity of each NLC cell is computed using $\sigma = L/RA$, which involves the sample thickness $L$, the sample area $A$, and the LC resistance $R$ acquired from the Nyquist curve. In the low-frequency region, in which the polarity of the applied electric field is preserved, impurity ions traverse a distance of d among the ITO electrodes during the transition time $t_{tr}$. The ionic mobility is described as [56]:

$$\mu = \frac{v}{E} = \frac{2d^2 f_{peak}}{\alpha V_0} \tag{8}$$

which involves the ions drift velocity ($v$), the electric field intensity ($E$), the effective voltage between the substrates ($V_0$), and $\alpha = C_{DL}/C_{LC}$ denoting the voltage attenuation coefficient inside the cell. Einstein's equation relates ion mobility to the diffusion coefficient [56]:

$$D = \frac{\mu K_B T}{e} \tag{9}$$

in which $k_B$ represents the Boltzmann's constant. The calculated parameters $\sigma$, $\mu$, $D$, and $\delta_N$ for NLC samples containing varied concentrations of ZnCdTeS QDs are presented in Table 2.

The resistivity of connections and electrodes $R_{CR}$ stays relatively steady as dopant concentration increases. For the pure LC sample, the resistivity of the bulk $R_{LC}$ is 2.02 MΩ. $R_{LC}$'s value drops when QDs are added and attains a minimum of 1.03 MΩ at 0.50 wt%, but it increases as QD concentration is further increased. The electrical conductivity $\sigma$ is inversely proportional to $R_{LC}$. As a reference, $\sigma$ of the pure E7 is determined to be $1.37 \times 10^{-9}$ S cm$^{-1}$. With increasing ZnCdTeS QDs concentration, the conductivity increases to $2.69 \times 10^{-9}$ S cm$^{-1}$ at 0.50 wt % but drops on the further increase. This remarkable 96% increase in conductivity owing to the inclusion of only 0.50 wt% non-conductive ZnCdTeS QDs suggests that the QDs provide new paths for charge transfer in the LC medium. This is consistent with the view that the anisotropic nematic environment favors the organization of QDs into ordered chain-like arrangements. The organized QDs arrays serve as direct channels for charge transport in the LC medium. The conductivity of an LC system can be controlled by varying ZnCdTeS QD concentration. This conductivity-tunable LC system can be advantageous for circuits operating in a susceptible system. The capacitance of bulk NLC $C_{LC}$ increases systematically with increasing QD concentration, as seen in Table 2. The rise in $C_{LC}$ indicates that the perpendicular component of the permittivity for LC samples increases as the QD concentration increases; hence, it implies that the connections between QD and LC molecules and the interaction between QDs improve. $C_{DL}$ of the LC cell rises on adding ZnCdTeS to 0.50 wt% and drops upon further addition of the QD. In a low-frequency region, when LC molecules at the interface interact with the QDs, a double layer emerges at the electrode and in the LC medium; therefore, increasing the ZnCdTeS QDs ratio increases the value of double-layer capacitance. In the low-frequency region, the double-layer capacitance predominates the impedance response since it is three orders of magnitude greater than $C_{LC}$. $W_{sr}$ reflects the resistivity of mobile ion diffusion from the bulk to the interface in the low-frequency region. Due to the fact that ZnCdTeS QDs interact with LC species, and ionic impurities prefer to reside on QDs rather than the electrode surface, increasing the QD ratio decreases the Warburg coefficient. The trend of variation in the ion diffusion coefficient $D$ and mobility $\mu$ is associated with the QDs' ion-capturing mechanism. It has been reported that the concentration of QDs could significantly affect the concentration and diffusion coefficient of mobile ions in a QD-doped NLC system [64]. The induced dipole moments of the QDs can effectively capture ions in the LC medium, enabling the residual ionic impurities to diffuse and transfer readily. The attendance of QDs as external additives may restrict the diffusion of ions, resulting in a drop in $D$ and $\mu$ when a lower concentration of QDs is introduced. In the doped systems, as the concentration of QDs increases, the ions trapped on the QDs surface rise, leading to an increase in ion diffusion coefficient and mobility. However, when higher concentrations of QD are introduced, aggregation development in the LC environment reduces the effective surface for the ion-trapping process, resulting in a drop in $D$ and $\mu$. The inclusion of ZnCdTeS QDs lowers the thickness of the Nernst diffusion layer $\delta_N$ in a doped LC system compared to the pure E7 sample. No correlation is observed between $\delta_N$ and the concentration of QDs in the doped samples.

## 4. Conclusion

In summary, the impact of ZnCdTeS QD doping on the electro-optic switching, dielectric, and electrochemical responses of the E7 NLC was studied. The dielectric analysis demonstrated that, in the nematic phase, when ZnCdTeS QDs are introduced to the NLC, $\varepsilon_{\parallel}$ increases more than $\epsilon_{\perp}$ owing to the creation of self-organized QD arrays along the nematic director and the increased order parameter. The value of $\Delta\epsilon$ enhanced as the concentration of QDs increased up to 0.50 wt% but then dropped when more QDs were added. Electro-optical measurements demonstrated that the doping of ZnCdTeS QDs reduces the $V_{th}$ and response time considerably. NLC containing ZnCdTeS QDs (0.50 wt%) exhibited a ~50% decrease in the optical switching-off time compared to pure NLC. ZnCdTeS QDs can efficiently capture ionic impurities, resulting in fewer ions adsorbing on the electrodes and diminishing the screening effect. Electro-optical properties were improved due to the swiping of the mobile ions by QDs, enhancement of LC-QD and QD-QD intermolecular interactions, and increase in dielectric anisotropy within the NLC system. The QDs provided novel channels for charge transfer in the LC medium, leading to an increase of ~96% in the NLC system's electrical conductivity. In addition, the introduction of ZnCdTeS QDs considerably enhanced the charge capacitance of the NLC device. We believe such QDs-NLC mixtures would be valuable for the next generation of tunable optoelectronic devices.

## CRediT authorship contribution statement

**Zahra Seidalilir:** Conceptualization, Methodology, Validation, Investigation, Data curation, Resources, Writing – original draft, Writing

**Table 2**
The obtained EEC model elements $R_{LC}$, $C_{LC}$, $C_{DL}$, and $W_{sr}$ based on the best fit and the calculated parameters $\sigma$, $\mu$, $D$, and $\delta_N$ for NLC cells containing varied concentrations of ZnCdTeS QDs.

| Samples | $R_{LC}$ (MΩ) | $C_{LC}$ (pF) | $C_{DL}$ (μF) | $W_{sr}$ (MΩ s$^{-0.5}$) | $\sigma$ ($10^{-9}$ S cm$^{-1}$) | $\mu$ ($10^{-10}$ m$^2$ s$^{-1}$ V$^{-1}$) | $D$ ($10^{-12}$ m$^2$ s$^{-1}$) | $\delta_N$ (μm) |
|---|---|---|---|---|---|---|---|---|
| None | 2.02 | 30.93 | 0.25 | 11.40 | 1.37 | 5.88 | 15.01 | 11.46 |
| 0.10 wt% QDs | 1.99 | 36.34 | 0.37 | 9.10 | 1.39 | 1.50 | 3.83 | 5.75 |
| 0.25 wt% QDs | 1.66 | 37.03 | 0.49 | 7.52 | 1.67 | 1.51 | 3.86 | 5.78 |
| 0.50 wt% QDs | 1.03 | 41.91 | 0.63 | 4.76 | 2.69 | 4.13 | 10.54 | 9.52 |
| 0.75 wt% QDs | 1.48 | 52.38 | 0.54 | 6.29 | 1.87 | 2.59 | 6.61 | 7.50 |
| 1 wt% QDs | 1.24 | 54.31 | 0.46 | 6.93 | 2.23 | 1.34 | 3.42 | 5.46 |

– review & editing. **Sepideh Shishehbor:** Validation, Investigation, Methodology. **Ehsan Soheyli:** Conceptualization, Validation, Investigation, Data curation, Writing – original draft, Writing – review & editing. **Mohammad Sabaeian:** Validation, Resources, Writing – review & editing.

## Declaration of competing interest

The authors declare that they have no known competing financial interests or personal relationships that could have appeared to influence the work reported in this paper.

## Data availability

No data was used for the research described in the article.

## Acknowledgements

Z. Seidalilir and E. Soheyli thank Professor Reza Sahraei from Ilam university for his assistance and guidance.

## Appendix A. Supplementary data

Supplementary data to this article can be found online at https://doi.org/10.1016/j.optmat.2023.113868.

## References

[1] D. Andrienko, Introduction to liquid crystals, J. Mol. Liq. 267 (2018) 520–541.
[2] P. Oswald, P. Pieranski, Nematic and Cholesteric Liquid Crystals: Concepts and Physical Properties Illustrated by Experiments, Taylor & Francis, 2005.
[3] C. Tschierske, Development of structural complexity by liquid crystal self-assembly, Angew. Chem. Int. Ed. 52 (34) (2013) 8828–8878.
[4] S.-J. Woltman, G.-D. Jay, G.-P. Crawford, Liquid-crystal materials find a new order in biomedical applications, Nat. Mater. 6 (2007) 929–938.
[5] J. Mather, L.P. Jones, P. Gass, A. Imai, T. Takatani, K. Yabuta, Potential improvements for dual directional view displays, Appl. Opt. 53 (2014) 769–776.
[6] C. Esteves, E. Ramou, A.R.P. Porteira, A.J.M. Barbosa, A.C.A. Roque, Seeing the unseen: the role of liquid crystals in gas-sensing technologies, Adv. Opt. Mater. 8 (2020), 1902117.
[7] A.K. Misra, B.P. Singh, S. Chandraker, K.K. Pandey, P.K. Tripathi, J.K. Saluja, R. Manohar, Faster response and lesser threshold voltage of strontium hardystonite (Sr-HT) nematic liquid crystal: photoluminescence and optical study, Opt. Mater. 93 (2019) 19–24.
[8] S.D. Durbin, S.M. Arakelian, Y.R. Shen, Optical-field-induced birefringence and Freedericksz transition in a nematic liquid-crystal, Phys. Rev. Lett. 47 (19) (1981) 1411–1414.
[9] C.P. Kumar, V. Sharma, P. Malik, K.K. Raina, Nano particles induced vertical alignment of liquid crystal for display devices with augmented morphological and electro-optical characteristics, J. Mol. Struct. 1196 (2019) 866–873.
[10] J.C. Choi, J.W. Lee, D.J. Lee, Y.K. Park, H.R. Kim, Flicker-free fringe-field switching liquid crystal display operable at extremely low frequencies for power saving, Adv. Eng. Mater. 23 (2021), 2100174.
[11] S.W. Jang, W. Choi, S. Kim, J. Lee, S. Na, S. Ham, J. Park, H. Kang, B.K. Ju, H. Kim, Complex spatial light modulation capability of a dual layer in-plane switching liquid crystal panel, Sci. Rep. 12 (2022) 8277.
[12] Y.F. Wang, Y.Q. Guo, Y.X. Ren, M.Z. Fu, J.L. Zhu, Y.B. Sun, Study on polyvinylidene fluoride as alignment layer in twist-nematic liquid crystal display, Liq. Cryst. 45 (2018) 857–863.
[13] S.J. Shivaraja, R.K. Gupta, S. Kumar, V. Manjuladevi, Enhanced electro-optical response of nematic liquid crystal doped with functionalised silver nanoparticles in twisted nematic configuration, Liq. Cryst. 47 (2020) 1678–1690.
[14] S.P. Yadav, M. Pande, R. Manohar, S. Singh, Applicability of $TiO_2$ nanoparticle towards suppression of screening effect in nematic liquid crystal, J. Mol. Liq. 208 (2015) 34–37.
[15] W.T. Chen, P.S. Chen, C.Y. Chao, Effect of doped insulating nanoparticles on the electro-optical characteristics of nematic liquid crystals, Jpn. J. Appl. Phys. 48 (2009), 015006.
[16] Y. Huang, P.J. Bos, A. Bhowmik, The ion capturing effect of 5° SiOx alignment films in liquid crystal devices, J. Appl. Phys. 108 (2010), 064502.
[17] T.R. Chou, J. Hsieh, W.T. Chen, C.Y. Chao, Influence of particle size on the ion effect of $TiO_2$ nanoparticle doped nematic liquid crystal cell, Jpn. J. Appl. Phys. 53 (2014), 071701.
[18] S. Hicks, S. Hurley, Y. Yang, D.K. Yang, Electric polarization frozen by a polymer network in nematic liquid crystals, Soft Matter 9 (2013) 3834.
[19] A. Maleki, Z. Seidali, M.S. Zakerhamidi, M.H.M. Ara, Dichroic ratio and order parameters of some Sudan dyes doped in nematic liquid crystalline matrix, Optik 126 (2015) 5473–5477.
[20] C.Y. Huang, P. Selvaraj, G. Senguttuvan, C.J. Hsu, Electro-optical and dielectric properties of $TiO_2$ nanoparticles in nematic liquid crystals with high dielectric anisotropy, J. Mol. Liq. 286 (2019), 110902.
[21] H. Eskalen, S. Ozgan, U. Alver, S. Kerli, Electro-Optical properties of liquid crystals composite with zinc oxide nanoparticles, Acta Phys. Pol., A 127 (2015) 756–760.
[22] G. Yadav, G. Pathak, K. Agrahari, M. Kumar, M.S. Khan, V.S. Chandel, R. Manohar, Improved dielectric and electro-optical parameters of nematic liquid crystal doped with magnetic nanoparticles, Chin. Phys. B 28 (2019), 034209.
[23] R. Vafaie, A. Vahedi, M.S. Zakerhamidi, H. Tajalli, Dielectric and electro optical properties of 6CHBT nematic liquid crystals doped with MgO nanoparticles, Liq. Cryst. 48 (2021) 1417–1428.
[24] J. Prakash, S. Khan, S. Chauhan, A.M. Biradar, Metal oxide-nanoparticles and liquid crystal composites: a review of recent progress, J. Mol. Liq. 297 (2020), 112052.
[25] B.P. Singh, S. Sikarwar, S. Tripathi, S. Agarwal, M. Sah, R. Manohar, K.K. Pandey, Thermodynamic and spectroscopic characterization of a weakly polar liquid crystalline compound dispersed with polyvinyl pyrrolidone capped gold nanoparticles, J. Mol. Liq. 354 (2022), 118889.
[26] W. Lee, C.Y. Wang, Y.C. Shih, Effects of carbon nanosolids on the electrooptical properties of a twisted nematic liquid-crystal host, Appl. Phys. Lett. 85 (2004) 513–515.
[27] R. Basu, Enhancement of polar anchoring strength in a graphene-nematic suspension and its effect on nematic electro-optic switching, Phys. Rev. E 96 (2017), 012707.
[28] S.K. Gupta, D.P. Singh, R. Manohar, S. Kumar, Tuning phase retardation behaviour of nematic liquid crystal using quantum dot, Curr. Appl. Phys. 16 (2016) 79–82.
[29] A.P. Litvin, I.V. Martynenko, F.P. Milton, A.V. Baranov, A.V. Fedorov, Y.K. Gun'ko, Colloidal quantum dots for optoelectronics, J. Mater. Chem. 5 (2017) 13252–13275.
[30] L. Yueyue, S. Siqi, W. Yilin, L. Fengmin, W. Hongtao, B. Jihao, L. Min, L. Geyu, $CsPbBr_3$ quantum dots enhanced ZnO sensing to $NO_2$ at room temperature, Sens. Actuators, B 368 (2022), 132189.
[31] J. Yao, P. Li, L. Li, M. Yang, Biochemistry and biomedicine of quantum dots: from biodetection to bioimaging, drug discovery, diagnostics, and therapy, Acta Biomater. 74 (2018) 36–55.
[32] R. Basu, G.S. Iannacchione, Evidence for directed self-assembly of quantum dots in a nematic liquid crystal, Phys. Rev. E 80 (2009), 010701.
[33] J. Mirzaei, M. Reznikov, T. Hegmann, Quantum dots as liquid crystal dopants, J. Mater. Chem. 22 (2012) 22350–22365.
[34] G. Singh, M. Fisch, S. Kumar, Emissivity and electro-optical properties of semiconducting quantum dots/rods and liquid crystal composites: a review, Rep. Prog. Phys. 79 (2016), 056502.
[35] G. Singh Supreet, Recent advances on cadmium free quantum dots-liquid crystal nanocomposites, Appl. Mater. Today 21 (2020), 100840.
[36] N. Atzin, O. Guzmán, O. Gutiérrez, L.S. Hirst, S. Ghosh, Free-energy model for nanoparticle self-assembly by liquid crystal sorting, Phys. Rev. E 97 (2018), 062704.
[37] Z. Seidalilir, E. Soheyli, M. Sabaeian, R. Sahraei, Enhanced electrochemical and electro-optical properties of nematic liquid crystal doped with Ni:ZnCdS/ZnS core/shell quantum dots, J. Mol. Liq. 320 (2020), 114373.
[38] N.A. Shurpo, M.S. Vakshtein, N.V. Kamanina, Effect of CdSe/ZnS semiconductor quantum dots on the dynamic properties of nematic liquid crystalline medium, Tech. Phys. Lett. 36 (2010) 54–59.
[39] R.K. Shukla, Y.G. Galyametdinov, R.R. Shamilov, W. Haase, Effect of CdSe quantum dots doping on the switching time, localised electric field and dielectric parameters of ferroelectric liquid crystal, Liq. Cryst. 41 (2014) 1889–1896.
[40] B. Kinkead, T. Hegmann, Effects of size, capping agent, and concentration of CdSe and CdTe quantum dots doped into a nematic liquid crystal on the optical and electro-optic properties of the final colloidal liquid crystal mixture, J. Mater. Chem. 20 (2010) 448–458.
[41] M.J. Cho, H.G. Park, H.C. Jeong, J.W. Lee, Y. Ho Jung, D.H. Kim, J.H. Kim, J. W. Lee, D.S. Seo, Superior fast switching of liquid crystal devices using graphene quantum dots, Liq. Cryst. 41 (2014) 761–767.
[42] A. Rastogi, K. Agrahari, G. Pathak, A. Srivastava, J. Herman, R. Manohar, Study of an interesting physical mechanism of memory effect in nematic liquid crystal dispersed with quantum dots, Liq. Cryst. 46 (2019) 725–735.
[43] M. Bouchakour, Y. Derouiche, Z. Bouberka, C. Beyens, L. Mechernène, F. Riahi, U. Maschke, Optical properties of electron beam- and UV-cured polypropyleneglycoldiacrylate/liquid crystal E7 systems, Liq. Cryst. 42 (2015) 1527–1536.
[44] A. Selevou, G. Papamokos, T. Yildirim, H. Duran, M. Steinhart, G. Floudas, Eutectic liquid crystal mixture E7 in nanoporous alumina. Effects of confinement on the thermal and concentration fluctuations, RSC Adv. 9 (2019) 37846–37857.
[45] E. Soheyli, S. Zargoush, A.F. Yazici, R. Sahraei, E. Mutlugun, Highly luminescent ZnCdTeS nanocrystals with wide spectral tunability for efficient color-conversion white-light-emitting-diodes, J. Phys. D Appl. Phys. 54 (2021), 505110.
[46] A. Ranjkesh, N. Ebrahimpour, M.S. Zakerhamidi, S.M. Seyedahmadian, Temperature-dependent dielectric property of a nematic liquid crystal doped with two differently–shaped tungsten oxide ($W_{18}O_{49}$) nanostructures, J. Mol. Liq. 348 (2022), 118024.
[47] M.S. Zakerhamidi, S. Shoarinejad, S. Mohammadpour, $Fe_3O_4$ nanoparticle effect on dielectric and ordering behavior of nematic liquid crystal host, J. Mol. Liq. 191 (2014) 16–19.

[48] G.K. Khushboo, P. Malik, Mesomorphic, electro-optic and dielectric behavior of self-assembled nanocomposite materials: nematic mixture doped with carbon coated cobalt nanoparticles, J. Mol. Liq. 351 (2022), 118639.
[49] C.W. Oh, E.G. Park, H.G. Park, Enhanced electro-optical properties in titanium silicon oxide nanoparticle doped nematic liquid crystal system, Surf. Coat. Technol. 360 (2019) 50–55.
[50] M. Schadt, Liquid crystal materials and liquid crystal displays, Annu. Rev. Mater. Sci. 27 (1997) 305.
[51] R. Basu, D.T. Gess, Electro-optic hybrid aligned nematic device utilizing carbon nanotube arrays and two-dimensional hexagonal boron nitride nanosheet as alignment substrates, Phys. Rev. E 104 (2021), 054702.
[52] R. Basu, L.J. Atwood, G.W. Sterling, Dielectric and electro-optic effects in a nematic liquid crystal doped with h-BN flakes, Crystals 10 (2020) 123.
[53] E. Jakeman, E.P. Raynes, Electro-optic response times in liquid crystals, Phys. Lett. 39A (1972) 69–70.
[54] R. Basu, A. Garvey, D. Kinnamon, Effects of graphene on electro-optic response and ion-transport in a nematic liquid crystal, J. Appl. Phys. 117 (2015), 074301.
[55] N.O. Laschuk, E.B. Easton, O.V. Zenkina, Reducing the resistance for the use of electrochemical impedance spectroscopy analysis in materials chemistry, RSC Adv. 11 (2021), 27925.
[56] B. Belyaev, N.A. Drokin, Impedance spectroscopy investigation of electrophysical characteristics of the electrode-liquid crystal interface, Phys. Solid State 57 (2015) 181–187.
[57] N. Dalir, S. Javadian, J. Kakemam, S.M. Sadrpoor, Enhance the electrical conductivity and charge storage of nematic phase by doping 0D photoluminescent graphene was prepared with small organicmolecule as a newarray quantum dot liquid crystal displays, J. Mol. Liq. 276 (2019) 290–295.
[58] J.H. Seo, J.W. Huh, H.J. Sohn, E. Lim, T.H. Yoon, Analysis of optical performance degradation in an ion-doped liquid-crystal cell with electrical circuit modeling, Crystals 10 (2020) 55.
[59] A. Serghei, M. Tress, J.R. Sangoro, F. Kremer, Electrode polarization and charge transport at solid interfaces, Phys. Rev. B 80 (2009), 184301.
[60] A.G. Garcia, R. Vergaz, J.F. Algorri, X. Quintana, J.M. Oton, Electrical response of liquid crystal cells doped with multi-walled carbon nanotubes, Beilstein J. Nanotechnol. 6 (2015) 396–403.
[61] G.J. Sprokel, Conductivity, permittivity, and the electrode space-charge of nematic liquid crystals. Part II, Mol. Cryst. Liq. Cryst. 26 (1974) 45–57.
[62] M. Urbanski, J.P.F. Lagerwall, Nanoparticles dispersed in liquid crystals: impact on conductivity, low frequency relaxation and electro-optical performance, J. Mater. Chem. C 4 (2016) 3485–3491.
[63] M. Xia, J. Nie, Z. Zhang, X. Lu, Z.L. Wang, Suppressing self-discharge of supercapacitors via electrorheological effect of liquid crystals, Nano Energy 47 (2018) 43–50.
[64] A. Rani, S. Chakraborty, A. Sinha, Effect of CdSe/ZnS quantum dots doping on the ion transport behavior in nematic liquid crystal, J. Mol. Liq. 342 (2021), 117327.